ACS Catalysis

Research Article

pubs.acs.org/acscatalysis

Engineering Gold Nanoparticles with DNA Ligands for Selective Catalytic Oxidation of Chiral Substrates

Pengfei Zhan, Zhen-Gang Wang,* Na Li, and Baoquan Ding*

National Center for Nanoscience and Technology, No. 11 BeiYiTiao, ZhongGuanCun, Beijing 100190, China

Supporting Information

ABSTRACT: Noble metal nanoparticles are promising materials for heterogeneous enantioselective catalysis because of their high surface-to-volume ratios, large concentrations of highly undercoordinated surface sites, and quantum confinement effects. In this work, we report on the use of DNA as an environment-responsive chiral ligand to engineer the selective catalytic behaviors of glucose oxidase-mimicking gold nanoparticles (AuNPs), with glucose enantiomers as the substrates. DNA can be stimulated externally to switch between random-coiled and multistranded structures (e.g., duplex, i-motif, or G-quadruplex). Random-coiled DNA-capped nanoparticles preferentially catalyze oxidation of L-glucose, and structured DNA-capped nanoparticles show higher activity toward D-glucose. pH-induced selectivity diminishment of DNA-treated AuNPs is also found, further demonstrating the chiral selector effect of DNA ligands. In the end, the selective catalysis of AuNPs allows control of the size enlargement of nanoparticles through self-catalytic Au^0 deposition, in ligand- and substrate chirality-dependent manners. It is found that the effect of substrate chirality on the self-growth rate can be reversed by the hybridization of the capping DNA. The structural and chemical features of DNA grooves in the multistranded structures render binding sites with higher affinity to D-glucose than L-glucose. The results suggest a simple strategy for engineering the responsive enantioselective catalysis of metallic nanoparticles and advance the understanding of chiral interactions between nucleic acids and saccharide.

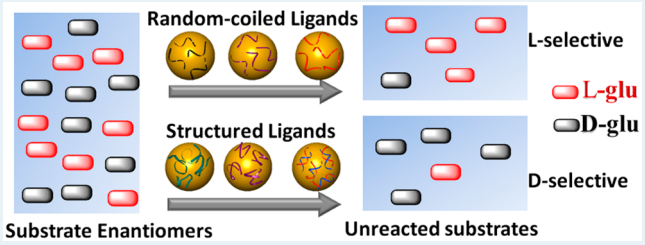

KEYWORDS: *gold nanoparticles, DNA, environmental responsiveness, catalysis, chiral selectivity*

INTRODUCTION

Chiral catalysis is a powerful approach to yield a chiral product,[1−5] or to differentiate between the two enantiomers of a racemic mixture.[6−10] For metal nanoparticle catalysts, surface functionalization with a chiral ligand is a simple strategy that offers the suitable stereochemical control over in a variety of reactions.[11−14] The configurational handedness of the capping ligands dominates the chiral selectivity of the catalytic nanoparticles through transferring the ligand asymmetry to the reactions. Progress in synthetic chemistry has enabled the design and synthesis of various metal nanoparticle-conjugated ligands with the desired chirality. It is noteworthy that the concept of using chirality-switchable ligands were proposed,[15,16] and such ligand-capped nanoparticles can respond smartly to the environmental conditions; however, the experimental employment of externally stimulated chirality-switchable ligands remains as a challenge for engineering the catalytic chiral selectivity of the metal nanoparticles.

The development of DNA nanotechnology provides a diversity of configurationally controllable molecules or structures.[17−19] DNA conformation can undergo the switch between random and multistranded states, triggered by environmental stimuli.[20−25] The stimuli-responsive features of DNA molecules are sequence-dependent and were used for various dynamic molecular devices, such as nanomachines[26,27] or sensors.[28] On the other hand, the helical structures endow DNA with intrinsic chirality. It enables DNA not only to be a selector for chiral recognition[29−35] but also to act as a scaffold for asymmetric catalysis.[36−38] Moreover, the chemical characteristics of the DNA structure entail the interaction of DNA with metal nanoparticles through coordination, such as gold nanoparticles (AuNPs).[39] AuNPs after treatment with DNA molecules still exhibit catalytic activity that is dependent on the DNA conformation.[40] This means the DNA molecules may behave like an optically active layer, which covers the catalytic metal nanoparticle and engineers the chiral catalysis to be responsive to the environmental change. Nevertheless, using DNA as the chirally selective ligands for the metallic nanocatalysts has not been reported. On the other hand, the DNA-guided biomimicking chiral catalysis also provides a simple means of studying the chiral recognition between DNA and the biological substrate (e.g., saccharide, peptide), which may provide valuable information on DNA−biological substance interactions.

Here, we choose AuNPs that can mimick glucose oxidase (GOx) as the model catalyst[41] and DNA molecules as the capping ligands to engineer the chiral selectivity of the nanocatalyst surface toward the glucose enantiomers, as schematically shown in Figure 1A (the redox routes catalyzed

Received: October 14, 2014
Revised: December 26, 2014
Published: January 22, 2015

DOI: 10.1021/cs5015805
ACS Catal. 2015, 5, 1489−1498

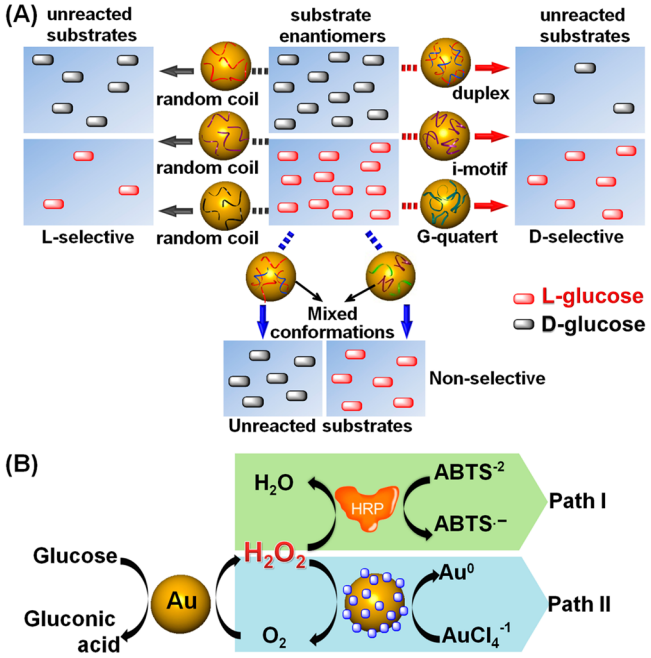

Figure 1. Schematic illustration of chiral differentiation between the glucose enantiomers by the catalytic DNA-capped AuNPs. (A) Left: AuNPs capped with single-stranded DNA random coils consumes L-glucose faster than D-glucose. Right: AuNPs capped with helically structured DNA consumes D-glucose faster than L-glucose. Down: AuNPs capped with mixed conformations shows nonselectivity to the substrate enantiomers. The states of the DNA are dependent on the environmental conditions and the sequences (marked in colors). (B) The enantiodifferentiation is performed through the catalytic oxidation of glucose by AuNPs that mimick the glucose oxidase. The produced H_2O_2 acts as the intermediate, either oxidizing $ABTS^{2-}$ to the colorimetric $ABTS^{-\bullet}$ catalyzed by HRP (path I) or reducing $AuCl_4^{-1}$ to Au^0 catalyzed by Au NP, resulting in the size enlargement (path II).

by AuNPs are shown in Figure 1B). DNA molecules interact with AuNP through multiple-point Au−N coordination[39,42] to form a chiral layer, in which the helically stacked bases of DNA molecules or the helical grooves provide the stereoselective recognition to the chiral biomolecules.[31,35,43] The recognition of saccharide to DNA helix through minor groove binding was also indicated.[43−45] Therefore, the molecular substrates (i.e., glucose) with specific chirality are allowed to approach the catalyst. The uncoordinated gold atoms on the nanoparticle surface act as the role to catalyze the H_2O_2 oxidation of glucose enantiomer substrates. In a sequence-dependent fashion, the conformation of DNA molecules is dependent on various environmental stimuli, such as pH change, the presence of the complementary strands or specific metal ions, switching between randomly coiled state and double-stranded or folded structures. In this work, DNA ligand-capped AuNPs are expected to show affinity to and catalyze the oxidation of the glucose substrates with matched chirality, through stereospecific hydrogen bonding and van der Waals interactions. The sequence-dependent and environment-responsive features of DNA ligands were used to engineer the chirality-selective catalysis of the DNA-treated AuNPs thoroughly, as schematically shown in Figure 1A. The DNA-induced chiral selectivity was also employed to control the size enlargement kinetics of the metallic nanoparticles, depending on the conformation of the capping DNA and the glucose substrate chirality. DNA is a promising ligand, not only because of the structural features, but also because of the commercial availability of various sequences. Through this work, we aim to provide insights into the environment-responsive catalytic selectivity over the chiral substrates and also to promote the understanding of DNA−saccharide chiral interactions that are an important issue in the biological field. As well, we think our work will contribute to the development of artificial nanoenzymes in the aspect of the function control.[46,47]

MATERIALS AND METHODS

Materials. 2-(*N*-Morpholino)ethanesulfonic (MES) acid sodium salt, MES acid hydrate, hydrogen peroxidase and 2,2′-azinobis(3-ethylbenzthiazoline-6-sulfonate acid) (diammonium salt, $ABTS^{2-}$) were purchased from Sigma-Aldrich. Glucose enantiomers, fructose enantiomers, mannose enantiomers, and galactose enantiomers were purchased from Aladdin Industrial Inc. All DNA oligonucleotides (purified with dual PAGE) and SYBR Gold nucleic acid gel stain were purchased from Invitrogen Life Technologies (Shanghai, China). $HAuCl_4$ and trisodium citrate were of analytical grade and used as received. Citrate-coated AuNPs with an average diameter of 5, 15, and 40 nm were prepared according to the citrate/$NaBH_4$ coreduction, citrate reduction, and seeded growth methods,[48] respectively. Concentration of the as-prepared AuNPs was determined with UV−vis spectroscopy using Lambert−Beer's law (molar extinction coefficient of 5, 15, and 40 nm AuNPs are 9.3×10^8 M^{-1} cm^{-1} at λ_{515}, 2.7×10^8 M^{-1} cm^{-1} at λ_{520}, and 8.42×10^9 M^{-1} cm^{-1} at λ_{530}).

Activity Assay. Required DNA strands with various concentrations were mixed with 16 nM of AuNPs in MES solution (25 mM, $[Na^+]$ = 18 mM, pH was adjusted by NaOH) at 15 °C. If hybridization was required, it was performed by slow cooling from 90 °C under the same buffer conditions before the mixing with AuNPs. After 10 min, 5 mM of L-glucose or D-glucose was added to the DNA−AuNPs mixture, which was further incubated at 25 °C for 30 min to generate the catalytic product, H_2O_2. Thereafter, AuNPs were removed from the mixture by centrifugation at 14 000 rpm for 15 min at 4 °C to eliminate the interference of AuNPs with the colorimetric reaction. HRP (0.05 μM) and 1 mM $ABTS^{2-}$ in MES buffer solution (100 mM, pH 7.2) were mixed with an equal volume of the supernatant, and the catalytic oxidation of $ABTS^{2-}$ was monitored at λ = 415 nm with UV−vis spectroscopy. UV−vis absorption spectroscopy was performed with a Shimadzu UV-2450 spectrophotometer. The pH of the reaction solution was measured with a Mettler-Toledo pH meter that was equipped with a microelectrode.

Surface Density Quantification of DNAon AuNPs. The DNA surface density was quantified according to the published protocol.[42,49] In this work, Cy5-labeled ssDNA (**1**) and dsDNA (**1**)/(**2**) of various concentrations (0−3.0 μM) was first adsorbed to 16 nM AuNPs for 10 min. Mercaptoethanol (ME) was mixed (final concentration 20 mM) to the fluorescently labeled DNA−AuNPs solution and incubated overnight at room temperature. Released DNA was separated via centrifugation (14 000 rpm), and the fluorescence was measured with a fluorescence spectrometer (F-4500, Hitachi, Tokyo, Japan). The molar concentration of DNA was determined by a standard linear calibration curve that was prepared with known concentrations of oligonucleotide with identical buffer pH, ionic strength, and ME concentration.

AuNPs Growth. The AuNPs enlargement experiments were implemented in 10 mM phosphate buffer saline ($[Na^+]$ = 18 mM), including 0.3 nM of AuNPs (bare or interacting with

DOI: 10.1021/cs5015805
ACS Catal. 2015, 5, 1489−1498

required ssDNA or dsDNA), 50 mM of glucose, and 0.1 mM of $HAuCl_4$. The growth process was continuously monitored at a time interval of 10 min until the absorbance reached the saturation.

TEM Measurements. The TEM samples were prepared by drop-casting 5 uL of the sample solution on a carbon-coated grid (400 mesh, Ted Pella). Before drop-casting, the grids were treated by a negative glow discharge using an Emitch K100X machine. After 10 min, the excess solution was removed from the grid using filter paper. To remove the salt, the grid was washed with a drop of water, and the excess water was removed using filter paper. A drop of the enlarged AuNPs solution was used to treat the grid, and the excess solution was removed. The grid was kept at room temperature to evaporate the remaining solution. TEM studies were conducted using a Tecnei G2-20S Twin (200 kV).

RESULTS AND DISCUSSION

AuNPs catalyze the oxidation of glucose to gluconic acid and the reduction of O_2 to H_2O_2; H_2O_2 can oxidize 2,2′-azino-bis(3-ethylbenzothiazoline-6-sulfonic acid) ($ABTS^{2-}$) to the colored product $ABTS^{\bullet-}$ (λ_{max} = 415 nm), which is mediated by horseradish peroxidase (path I). This coupled reaction allowed probing the catalytic activity of AuNPs spectroscopically. The oxidation rate of glucose, defined as the GOx-mimicking activity of AuNPs, is proportional to the generation rate of H_2O_2. Because AuNPs were removed by ultracentrifugation prior to the addition of HRP and excessive $ABTS^{2-}$ was used, the concentration of the yielded H_2O_2 following glucose oxidation (within certain time) can be detected by monitoring the production of the colorimetric $ABTS^{\bullet-}$. Therefore, the catalytic activity of AuNPs is indicated as the HRP-catalyzed absorbance change at 415 nm (ΔA) of the reaction solution. It should be noted that in the centrifugation process, the chemical stability of H_2O_2 was concerned because of the potential of photo- or thermally induced decomposition. As a control experiment, we monitored the concentration of H_2O_2 in the solution containing only H_2O_2 in a range of concentrations (50 nM to 10 μM) at 240 nm (extinction coefficient: 40 mM^{-1} cm^{-1}). The implementation of the centrifugation process above did not change the concentrations of H_2O_2, demonstrating the stability of H_2O_2 in the experimental condition. On the other hand, the produced H_2O_2 from the GOx-mimicking catalytic reaction reduces the $AuCl_4^-$ to Au^0 with the catalytic AuNPs and enlarges the nanoparticles (path II). The rate of seeded growth is dependent on the GOx-mimicking catalytic activity of the AuNP seeds. The coupled redox reactions are schematically shown in Figure 1B.

Hybridization-Dependent Chiral Selectivity. We first investigated catalytic activity of the unmodified AuNPs (as-prepared citrate-coated AuNPs) in the presence of D-glucose and L-glucose, respectively. We found the activity toward the two substrate enantiomers was identical, indicating that the catalytic AuNP surface was incapable of differentiating the racemic glucose substrates (Supporting Information Figure S1). To engineer the selective catalytic behaviors of AuNPs, single-stranded DNA (ssDNA) and double-stranded DNA (dsDNA) were respectively used to interact with AuNPs. Both ssDNA and dsDNA can adsorb onto AuNPs through Au−N coordination, despite different affinities.[39] Figure 2A indicated the GOx-mimicking activity of AuNPs treated by ssDNA (**1**), the sequence of which is shown in Table 1 (other sequences of the capping DNA in this work are also included). The absorbance change (ΔA) resulting from the HRP-mediated oxidation of $ABTS^{2-}$

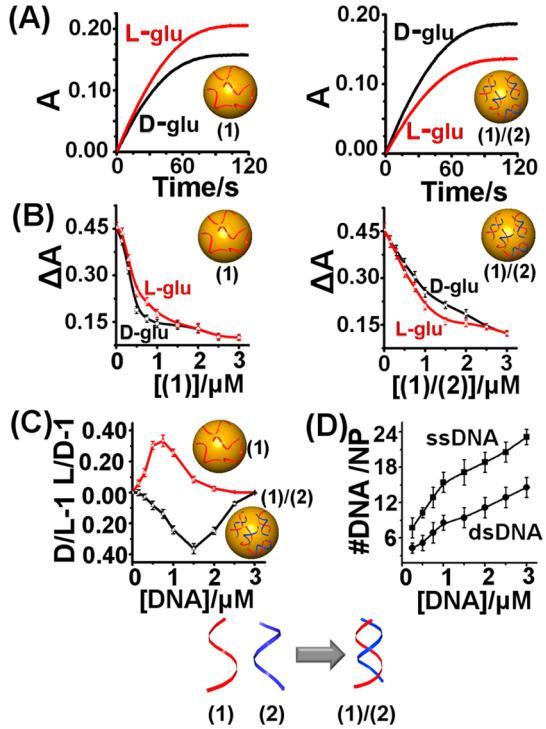

Figure 2. Hybridization-engineered chiral differentiation between the substrate enantiomers. (A) Time-dependent absorbance change of $ABTS^{\bullet-}$ upon treating AuNPs with ssDNA (**1**) (left, 0.75 μM) and dsDNA (**1**)/(**2**) (right, 1.5 μM), respectively. It indicates the hybridization-dependent selective catalysis behaviors of the treated AuNPs. (B) Environmental DNA concentration-dependent chiral catalytic selectivity of the AuNPs treated with ssDNA (**1**) (left) and dsDNA (**1**)/(**2**) (right). (C) Consumption excess of glucose enantiomers catalyzed by the (**1**)- and (**1**)/(**2**)-treated AuNPs, calculated from part B. (D)Surface coverage densities of dsDNA or ssDNA on each nanoparticle at different concentrations of the corresponding DNA-treated AuNPs (16 nM). The fluorescence data are shown in Supporting Information Figure S2 .

Table 1. Sequences of the capping DNA ligands

number	sequence
(**1**)	5′-CCCTAACCCTAACTCTAACCC-3′
(**2**)	5′-GGGTTAGAGTTAGGGTTAGG-3′
(**3**)	5′-CCCTAACCCTAACCCTAACCC-3′
(**4**)	5′-GGGTTAGTGTTAGTGTTAGGG-3′
(**5**)	5′-GGGTTAGGGTTAGGGTTAGGG-3′
(**6**)	5′-GGTTGGTGTGGTTGG-3′

arose solely from the AuNPs-catalyzed oxidation of glucose. Larger ΔA reflects the higher amount of H_2O_2 produced by AuNP catalysis within certain reaction time, thus, a higher GOx-mimicking activity of AuNPs. Because all the substrates but glucose in the coupled reactions were achiral, the absorbance change also reflects the catalytic selectivity of AuNPs toward the chiral glucose substrates.

(**1**)-Treated AuNPs indicated significantly higher catalytic activity toward L-glucose than D-glucose. It illustrated that the ssDNA-treated surface, on which the chirality was transferred from ssDNA molecules, preferred to approach and catalyze the oxidation of L-glucose. In other words, the surface-adsorbing ssDNA had much stronger interaction with L-glucose. ssDNA has a special stereo orientation that arises from chiral stacking of D-nucleosides, and H-bonding is an important factor to influence

DOI: 10.1021/cs5015805
ACS Catal. 2015, 5, 1489−1498

its interaction with other molecules.[34,35] Thus, it may have different abilities to form an effective physical interaction with the glucose enantiomers, which also has a strong capability to form H-bonds. The chirality and stereoselective effect entail the stronger affinity of ssDNA-treated AuNPs surface to L-glucose, which resulted in a higher oxidation rate of L-glucose than D-glucose. Moreover, the difference between the catalysis rate of L-glucose and D-glucose was found to be dependent on the environmental DNA concentration that treated the AuNPs, as shown in Figure 2B. When the DNA concentration was ∼0.75 μM, the treated AuNPs showed the optimal chiral selectivity, as shown in Figure 2C. It is also seen that the higher amount of DNA treating the AuNPs enhanced the surface passivation, indicating the noncoordinating gold atoms played a major role in the catalysis. The concentration-dependent catalytic activity and chiral differentiation reflected that the selective catalysis relied on the effective glucose−ssDNA interactions concerning the chiral recognition, and glucose−AuNPs interactions concerning the catalysis. The increase in the concentration of the treating DNA resulted in the increased surface coverage of DNA ligands on the AuNPs (Figure 2D). At low surface coverage, only a small amount of glucose enantiomers that approached the gold surface could be selectively oxidized. When the surface was fully covered by the DNA molecules, most of the substrate molecules were unable to reach the Au surface efficiently because of the steric hindrance. These two situations reduced the catalytic resolution of the glucose substrate enantiomers, which also demonstrated the role of ssDNA molecules in the chiral selectivity.

When AuNPs were treated by duplex (**1**)/(**2**) consisting of ssDNA (**1**) and its complementary strand (**2**), the chiral selectivity toward the substrate enantiomers was reversed, as indicated in Figure 2A. D-Glucose was oxidized faster than L-glucose under the catalysis of dsDNA-treated AuNPs, and the selectivity was also dependent on the concentration of dsDNA treating AuNPs (Figure 2B). The dsDNA concentration at the optimal selectivity was ∼1.5 μM (Figure 2C), higher than ssDNA, indicating a higher environmental DNA concentration could result in the comparable surface coverage of dsDNA to ssDNA (note: the surface coverage density at the optimal selectivity for dsDNA and ssDNA was 9 and 12 for each nanoparticle (Figure 2D), which was calculated from Figure S2). This is due to weaker adsorption of dsDNA (compared with ssDNA) to AuNPs, resulting from the stronger electrostatic repulsion between dsDNA and AuNPs.[39] The chirality of dsDNA originates from its helical conformation, different from that of ssDNA from the stacking of bases. The differential catalysis indicated that the nucleosides in the right-handed helix had a higher affinity in D-glucose than in L-glucose, which was a chirality transfer from helical DNA to the catalytic reaction. The selectivity factor (S) was 1.333 for ssDNA-treated AuNPs ($k_{\text{L-glucose}}/k_{\text{D-glucose}}$) and 1.367 for dsDNA-treated AuNPs ($k_{\text{D-glucose}}/k_{\text{L-glucose}}$).

In addition to the DNA ligand concentration and conformation, we investigated the effect of the sequence specificity, sequence length, and DNA-coating temperature on the chiral selectivity of treated AuNPs. It was found that the chiral selectivity was affected by the nucleic sequence specificity. AuNPs treated by single-stranded DNA rich in thymine and cytosine showed a higher optimal selectivity than guanine and adenine bases (Supporting Information Figure S3) toward glucose enantiomers. AuNPs treated by the double-stranded DNA poly(A•T)$_{19}$, showed lower chiral selectivity than dsDNA rich in cytosine and guanine bases (i.e., (**1**)/(**2**)), and the opposite of single stranded poly(A)$_{19}$ and poly(T)$_{19}$. These indicated DNA ligands of various sequences were available to the hybridization-caused catalysis selectivity reversion.

To investigate the effect of the sequence length of the ligand on the chiral selectivity, we designed another two DNA strands that had a sequence similar to but longer than (**1**). As shown in Supporting Information Figure S4, as the sequence length increased, the optimal selectivity decreased, but not significantly. Moreover, the sequence length did not change the catalytic activity of the AuNPs. It is probably because the increase in the ligand length could not enable each nucleotide to interact with the AuNP surface efficiently. We also investigated the chiral selectivity of AuNPs treated by DNA ligands shorter than (**1**) and mononucleotides (adenosine triphosphate (ATP), thiamine triphosphate (TTP), cytidine triphosphate (CTP) or guanosine triphosphate (GTP)). The results are shown in Figure S5 and Figure S6. It is found that the decrease in the base number of the DNA ligand enhanced the catalytic activity while reducing the chiral selectivity of the treated AuNPs significantly. Such ligand-length-dependent chiral selectivity may further demonstrate the role of the base stacking of ssDNA in the enantiodiscrimination between the glucose enantiomers, rather than the asymmetric deoxyribose. The reduction in the stacking effect, resulting from the reduced length of the DNA ligands, decreased the chiral selectivity of the catalytic AuNPs toward L- and D-glucose.

The temperature may also be an important factor that affects the chiral selectivity of the DNA-treated AuNPs, through the intramolecular hydrogen bonding (related to the secondary structure) and the coordination to AuNPs. High temperature favors the coordination of DNA to AuNPs but can damage the hydrogen bonding, and low temperature can do the opposite. The temperature at which AuNPs were treated by DNA (**1**) was varied from 5 to 35 °C, and the temperature did not exhibit a significant effect on the catalytic selectivity (Supporting Information Figure S7).

It should also be noted that free-diffusing DNA ligands that did not adsorb to AuNPs may also affect the chiral selectivity of the catalytic treated AuNPs. To demonstrate the role of the free ligands in the selectivity toward glucose enantiomers, a control experiment was implemented in which prior to the addition of glucose to the DNA−AuNPs system, free DNA ligands were removed from the AuNPs by centriguation at 14 000 rpm until negligible DNA concentration was detected with UV absorption at 260 nm. The catalysis results are shown in Figure S8. The selectivity factor (S) was 1.342 for the ssDNA-treated AuNPs, similar to that in the presence of free DNA ligands (S = 1.333). It indicated that the chiral selectivity was mainly ascribed to the chiral DNA layer adsorbing on the AuNPs.

It is interesting that DNA-treated AuNPs also exhibited catalytic activity of mannose oxidase, galactose oxidase, and fructose oxidase, shown in Figure S9. The activity assays followed the procedures that assayed the GOx-mimicking activity of AuNPs. It was found that DNA (**1**)- and DNA (**1**)/(**2**)-treated AuNPs showed higher catalytic activity toward L- and D-monosaccharides (mannose, galactose, or fructose), respectively, similar to catalytic selectivity of GOx-mimicking DNA-treated AuNPs. It is noted that the selectivity of the ssDNA- or dsDNA-treated AuNPs toward glucose enantiomers was higher than that toward mannose, galactose, and fructose enantiomers, which implies the enantiodiscrimination of DNA between glucose enantiomers was more significant than the used monosaccharide enantiomers.

DOI: 10.1021/cs5015805
ACS Catal. 2015, 5, 1489−1498

The size effect of AuNPs with ssDNA (**1**) or dsDNA (**1**)/(**2**) as ligands on the chiral catalytic selectivity toward glucose enantiomers was investigated, as shown in Figure S10; 5, 15, and 40 nm AuNPs were used. The optimal selectivity factors for 15 nm AuNPs that were treated by ssDNA and dsDNA were slightly higher than 5 and 40 nm AuNPs. It was also found that as the size of the AuNPs increased, the optimal selectivity ($[DNA]_{opt}$) was achieved at higher concentrations of ssDNA or dsDNA ligands. This is because on the larger catalytic surface, more ligands are required for the optimal cooperation between the ligands and the surface in the aspect of the chiral selectivity.

pH Responsiveness-Dependent Chiral Selectivity. At pH 7.2, DNA (**3**) adopted the unfolded conformation; thus, (**3**)-covered AuNPs catalyzed the oxidation of L-glucose faster than D-glucose, with the optimal selectivity factor as 1.398 ($k_{L\text{-glucose}}/k_{D\text{-glucose}}$). At pH 5.2, DNA (**3**) existed as the folded i-motif, and the i-motif-treated AuNPs showed catalytic selectivity of D-glucose over L-glucose, with the optimal selectivity factor as 1.393 ($k_{D\text{-glucose}}/k_{L\text{-glucose}}$), as shown in Figure 3. In the control

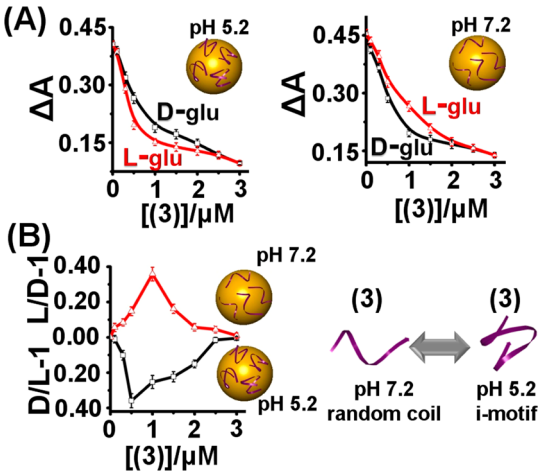

Figure 3. pH-engineered chiral differentiation between the substrate enantiomers based on pH-dependent conformations of the DNA ligands. (A) Environmental DNA concentration-dependent chiral selectivity of the AuNPs treated with DNA (**3**) at pH 5.2 (left) and pH 7.2 (right). (B) Consumption excess of glucose enantiomers catalyzed by the (**3**)-treated AuNPs at pH 5.2 and pH 7.2. DNA (**3**) adopts the i-motif conformation at pH 5.2 and random-coiled state at pH 7.2.

experiment, the uncoated AuNPs did not exhibit the selectivity over the glucose enantiomers at pH 5.2 (Supporting Information Figure S1). This indicates that the acidification of solution pH reversed the chiral selectivity of the (**3**)-treated AuNP catalyst. The catalytic selectivity for both the acidic and neutral solutions was found to be dependent on the concentration of DNA (**3**) that treated the AuNPs. At the optimal selectivity, the DNA concentration at pH 5.2 was lower than at pH 7.2. The acidification could promote the adsorption of DNA (**3**) to the AuNPs,[50,51] resulting in a higher coverage of the i-motif structures on the AuNPs than the unfolded strands. To verify that the pH-induced reversion of the catalysis selectivity was due to the intramolecular folding of the DNA, a DNA molecule that had a sequence analogous to (**3**) was used to treat AuNPs at pH 5.2 and pH 7.2 (exemplified by DNA (**1**)). This strand was unable to fold into the i-motif structure after environmental acidification, and the result indicates that the treated AuNPs showed catalytic preference to L-glucose at both acidic and neutral pH, demonstrating the role of the conformational change.

To further engineer the pH-based selective catalysis behavior, a strand (**4**) that could hybridize to (**3**) was introduced into the pH-based system. The sequence of DNA (**4**) was designed in such a way that (i) the number of complementary bases between (**4**) and (**3**) should yield a stable duplex structure; (ii) the number of complementary bases should also be limited so that (**4**) can be released upon the formation of the i-motif structure. The pH-triggered i-motif exhibits an enhanced stability as compared with the duplex stability of (**3**)/(**4**) ($\Delta G^0_{i\text{-motif}} = -19$ kcal/mol vs $\Delta G^0_{duplex} = -12$ kcal/mol).[24] Therefore, at neutral pH (pH 7.2), the mixed strands (**3**) and (**4**) behaved as a duplex, and (**3**)/(**4**)-treated AuNPs had higher catalytic activity toward D-glucose than L-glucose (Figure 4A). At acidic pH (pH 5.2), the

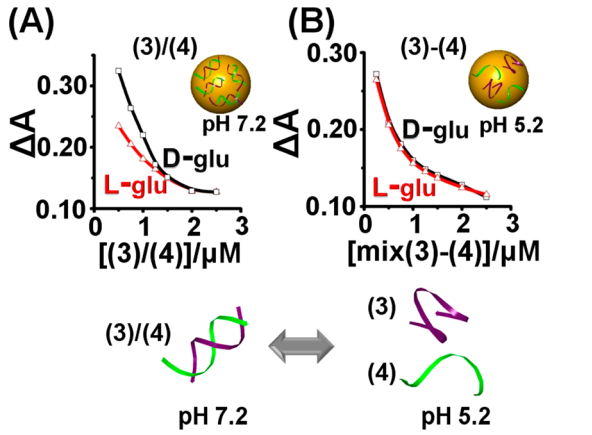

Figure 4. Chiral selectivity of AuNPs treated with DNA (**3**)/(**4**) at pH 7.2 (A) and 5.2 (B). At pH 7.2, the DNA strands hybridized to each other, resulting in the catalyzed oxidation of D-glucose faster than L-glucose. At pH 5.2, (**3**)/(**4**) adopted the separated i-motif and random-coiled states, behaving like a racemic mixture for the enantiomeric substrates and resulting in chiral selectivity diminishment of the treated AuNPs.

AuNPs were capped by the separated folded (**3**) (Figure 3) and randomly coiled (**4**) (Supporting Information Figure S11) that had a higher affinity to D- and L-glucose, respectively; thus, (**3**)/(**4**)-treated AuNPs indicated no preferential selectivity toward either of the substrate enantiomers, as shown in Figure 4B. Herein, (**3**) and (**4**) as the capping ligands behaved like the racemic mixtures that covered the AuNPs' surface: no selective affinity to the enantiomeric targets. It is concluded that the hybridization of the pH-responsive capping ligand transformed the pH-induced turnover behavior of the catalytic selectivity into the pH-induced diminishment behavior of the selectivity.

DNA–Glucose Affinity. The catalysis results provided indirect evidence for the chiral affinity of random-coiled or multistranded DNA to glucose enantiomers. For further verification, a competitive binding method was designed to investigate the enantiodiscrimination of DNA between L-glucose and D-glucose. In detail, a nucleic acid gel stain, SYBR Gold, was chosen to interact with the DNA ligands (**1**), (**1**)/(**2**), and (**3**) at acidic and neutral pH, respectively. Then either of the glucose enantiomers was mixed with and dissociated DNA–SYBR Gold complex. The competition methods were used to determine the binding affinity of DNA to a variety of small molecules, such as quinacrin,[52] actinomycine,[52] and porphyrin dimer.[53] SYBR Gold, purchased from Life Technologies, can exhibit >1000-fold

DOI: 10.1021/cs5015805
ACS Catal. 2015, 5, 1489–1498

fluorescence enhancement upon binding to nucleic acids; is much more sensitive than the commonly used DNA stain dyes, such as SYBR Green and ethidium bromide; and has been used for sensitive fluorescence detection of DNA aptamer substrates.[54] That is to say, the dissociation of SYBR Gold dye from DNA can result in a significant fluorescence decrease in the DNA−SYBR Gold complex.

As seen from Figure 5 (for the original fluorescence spectra, see Figure S12), either of the glucose enantiomers could result in

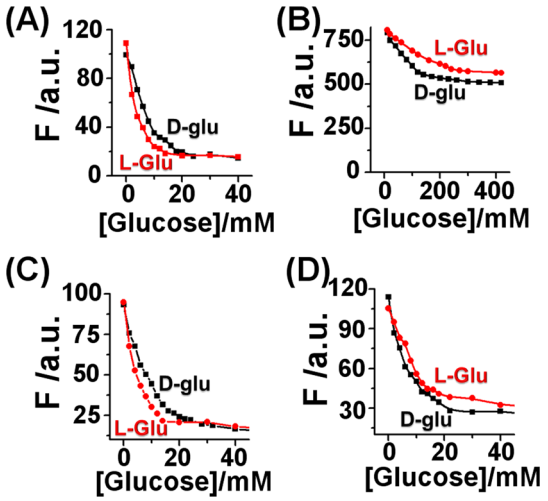

Figure 5. Glucose concentration-dependent fluorescence quenching of DNA−SYBR Gold complex. (A) ssDNA (**1**)−SYBR Gold complex. (B) dsDNA (**1**)/(**2**)−SYBR Gold complex. (C) ssDNA (**3**)−SYBR Gold complex at pH 7.2. (D) i-Motif DNA (**3**)−SYBR Gold complex at pH 5.2. Competition binding conditions: [DNA] = 1.0 μM, [SYBR Gold] = 0.1x concentration (10^5 dilution of the stock concentrate). DNA was first mixed with SYBR Gold and glucose for 10 and 20 min, respectively. The corresponding fluorescence spectra are seen in Figure S12.

the fluorescence quenching of the DNA−SYBR Gold complex, which was dependent on the glucose concentration and illustrated that glucose at an appropriate concentration could desorb SYBR Gold from the complex; however, this dependence was correlated to the DNA conformations. A much higher concentration of glucose was required to quench the fluorescence of dsDNA−SYBR Gold than ssDNA−SYBR Gold. This is because dsDNA can form a stronger complex with the dye, which was also reflected by the higher fluorescence intensity.

On the other hand, randomly coiled (**3**)−SYBR Gold and multifolded imotif (**3**)−SYBR Gold showed a comparable fluorescence intensity, and the concentrations of glucose required to quench these two complexes were similar, which may be because the SYBR Gold complexation with DNA was lower at acidic pH. From the results (Figure 5), it was found that L-glucose dissociated the dye from the randomly coiled DNA-based complex faster than multistranded DNA (dsDNA and i-motif)-based complexes, and D-glucose caused the dissociation of multistranded DNA-based complexes more significantly. This indicates DNA at randomly coiled and structured conformations showed a higher affinity toward L-glucose and D-glucose, respectively, which is consistent with what was concluded from the chirality selectivity-based catalysis.

Kinetics of the Catalysis. The kinetic parameters for AuNP-catalyzed oxidation of glucose, maximum reaction rates (V_{max}), and Michaelis−Menten constants (K_m), were used to further evaluate the selective catalysis of the treated AuNPs toward L-glucose and D-glucose. The kinetic parameters are shown in Table 2 and were determined from a double-reciprocal plot

Table 2. Kinetic Parameters of (1)−AuNPs, (1)/(2)−AuNPs, (3)−AuNPs at pH 5.2 and pH 7.2 with Glucose Enantiomers as the Substrate[a]

	substrate	V_{max} (A)	K_m (mmol L^{-1})
(**1**)−AuNPs	L-glu	0.216	0.0698
	D-glu	0.1863	0.0946
(**1**)/(**2**)−AuNPs	L-glu	0.1601	0.089
	D-glu	0.203	0.061
(**3**)−AuNPs pH5.2	L-glu	0.216	0.0698
	D-glu	0.1863	0.0946
(**3**)−AuNPs pH 7.2	L-glu	0.1601	0.089
	D-glu	0.203	0.061

[a] K_m = Michaelis−Menten constant. V_{max} = maximum reaction rate (represented by the absorbance change of the product $ABTS^{\bullet-}$).

(Lineweaver−Burk method) illustrated in Figure S13 (Supporting Information). A higher K_m reflects the lower affinity of the catalyst to the substrate, which is due to a stronger DNA−substrate interaction. Table 2 indicated that DNA-treated AuNPs exhibited different K_m values toward the glucose enantiomers. ssDNA (**1**)-treated AuNPs showed a lower K_m value toward L-glucose than D-glucose, whereas a lower K_m toward D-glucose than L-glucose was observed for dsDNA (**1**)/(**2**)-treated AuNPs. Both K_m and V_{max} values revealed that the hybridization of the capping DNA caused the reversion of the catalytic chiral selectivity. Similarly, AuNPs that were treated by DNA (**3**), showed a lower K_m and higher V_{max} values toward L-glucose at pH 7.2, but higher K_m and lower V_{max} values toward L-glucose at pH 5.2. This was attributed to the acidification-induced conformational folding of DNA (**3**). It indicated that i-motif-treated AuNPs had an affinity to the substrate enantiomers that was opposite to the random coil-treated AuNPs.

G-Quadruplex-Dependent Chiral Selectivity. The intermolecularly (duplex) and intramolecularly (i-motif) multistranded DNA structures resulted in similar chirality-based selective catalytic behaviors of treated AuNPs and opposite to single-stranded random coils. It is reasoned that the existence of grooves between the strands might differentiate the surface affinity to the glucose enantiomers. To test this hypothesis, another common four-stranded DNA motif was used to treat AuNPs.

In the presence of Na^+, guanine-rich DNA (**5**) was folded into the G-quadruplex,[38] in which four guanine bases associated into a guanine tetrad stacking on top of each other. As shown in Figure 6A, the G-quadruplex-treated AuNPs exhibited higher catalytic activity toward D-glucose, analogous to duplex and i-motif (S value at optimal selectivity was 1.297, $k_{D\text{-glucose}}/k_{L\text{-glucose}}$). As a comparison, AuNPs treated by strands with a similar G-rich sequence (**6**), which folded much less efficiently in the presence of Na^+,[55,56] showed chiral selectivity analogous to the aforementioned random-coiled strands (S value at optimal selectivity was 1.498, $k_{L\text{-glucose}}/k_{D\text{-glucose}}$), as shown in Figure 6B. The CD spectra of the DNA ligands (**5**) and (**6**) in the presence of Na^+ are shown in Figure 6C, indicating the dependence of G-quadruplex formation on the ligand sequence.

For time-dependent absorbance change (at 415 nm) caused by the catalysis of all treated AuNPs, see Supporting Information Figure S14.

DOI: 10.1021/cs5015805
ACS Catal. 2015, 5, 1489−1498

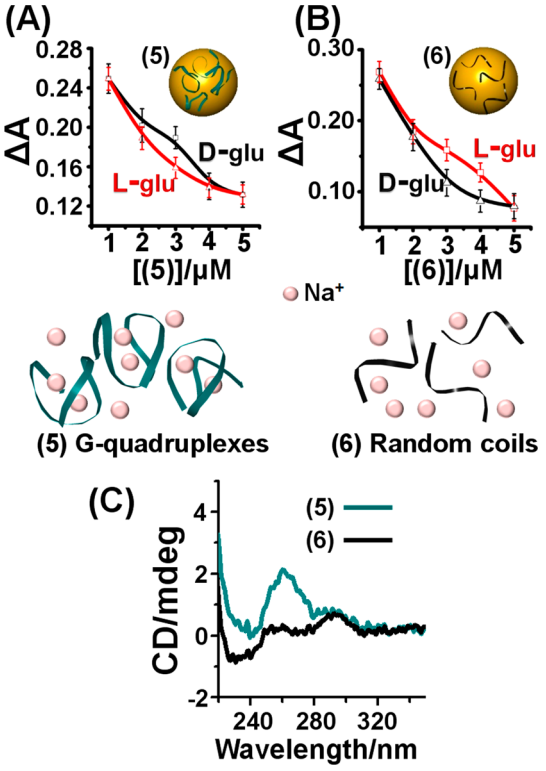

Figure 6. DNA folding-dependent catalytic chiral selectivity of AuNPs. In the presence of Na^+, (A) DNA (**5**) (green) folds itself into G-quadruplex that leads to higher affinity to D-glucose, (B) while DNA (**6**) (black), also rich in guanine bases, adopts the random-coiled conformation that has a higher affinity to L-glucose. (C) CD spectra of DNA (**5**) (1 μM) and (**6**) (1 μM) in the presence of Na^+.

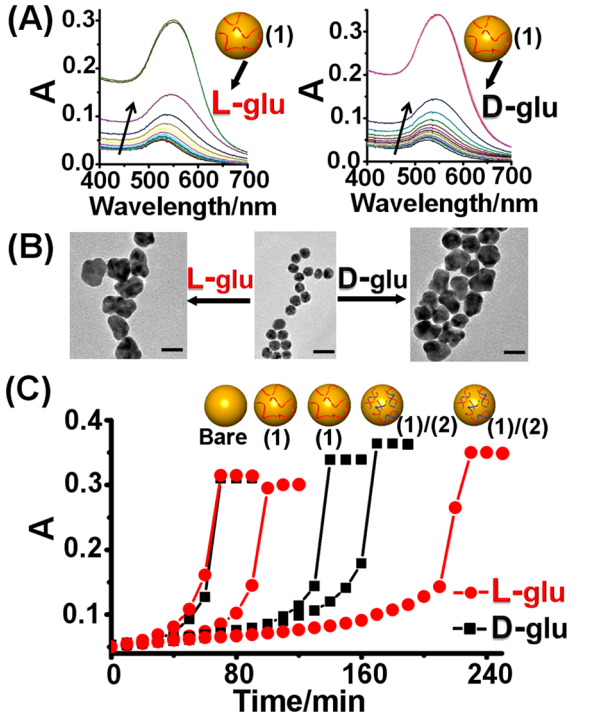

Figure 7. Growth of DNA-treated AuNPs. (A) Time-evolved UV–vis spectra of AuNPs treated by ssDNA (**1**) in the growth solution containing 50 mM glucose (left:, L-glucose; right, D-glucose). Time interval: 10 min. (B) TEM images of (**1**)-treated AuNPs before growth and after enlargement when subjected to L-glucose and D-glucose, respectively. The substrate chirality did not affect the shape and size of the enlarged nanoparticles. (C) Time-resolved plasmonic absorbance change (at 524 nm) that records the enlargement of AuNPs treated with (**1**) or (**1**)/(**2**) and subjected to L-glucose or D-glucose. It reveals the ssDNA-treated AuNPs grew faster when subjected to L-glucose than D-glucose, dsDNA–AuNPs grew faster in D-glucose than in L-glucose, and bare AuNPs grew at identical rates in D-glucose and in L-glucose. Scale bar: 25 nm.

Chiral Selectivity-Dependent AuNPs Enlargement. Great efforts have been focusing on the size and morphology control of noble metal nanoparticles through seeded synthesis.[57−60] Our endeavors in engineering of the differential AuNP catalysis could provide a novel strategy to control the seeded-growth kinetics of metal nanoparticles through the responsive conformation of the capping ligands. H_2O_2 that is generated during the glucose oxidase-mimicking AuNPs catalysis can be used to reduce $AuCl_4^{-1}$ to Au^0 with AuNP as seeds and to enlarge the metallic catalytic seeds.[61] Herein, AuNPs also act as the catalyst for H_2O_2 reduction of $AuCl_4^-$ reduction and Au^0 deposition. Consequently, the growth rate of the nanoparticle seeds is expected to be correlated to the GOx-mimicking catalytic activity of AuNPs.

To study the effect of substrate chirality on the growth rate of AuNP seeds, ssDNA (**1**) and dsDNA (**1**)/(**2**) were selected to cover AuNPs because they showed opposite chiral selectivity toward the substrate enantiomers. UV–vis spectroscopy was used to monitor the catalytic growth of AuNPs in real time, shown by the evolution of the plasmon absorbance spectra in Figure 7A. The time-dependence curves were plotted according to the absorbance spectra, with a time interval of 10 min. We first investigated the catalysis of (**1**)-treated AuNPs toward L-glucose. A gradual increase in the absorbance intensity was observed initially, suggesting the slow growth of AuNPs. Meanwhile, the red solution gradually changed to purple. At ~100 min, the absorbance reached the saturation value abruptly, and no further growth was observed after this point, indicating a feature of self-limited growth for the catalytic enlargement of AuNPs.[62] The self-limit is ascribed to two factors that inhibit the catalysis: the increased size slows down the catalysis rate, and the deposition of the product gluconic acid blocks the reactive Au atoms.[62]

The (**1**)-treated AuNPs catalyzed oxidation of D-glucose also resulted in self-limited growth of the nanoparticles (Figure 7A). However, the growth was much slower than that with L-glucose as the substrate, ~140 min to reach the saturated absorbance, at which AuNPs showed size and shape similar to L-substrate-enlarged nanoparticles (Figure 7B). It implied the optical activity of the substrate for GOx-mimicking catalysis affected the growth rate of the AuNP seeds, which was attributed to the selective catalytic oxidation of the substrate enantiomers. The differential growth of the nanoparticles was further demonstrated by dsDNA (**1**)/(**2**)–AuNPs' catalyzed oxidation of the substrate enantiomers, as shown in Supporting Information Figure S15. As afore demonstrated, (**1**)/(**2**)–AuNPs showed higher catalytic activity toward the oxidation of D-glucose than L-glucose. The growth rate of (**1**)/(**2**)–AuNPs with D-glucose as the substrate was substantially faster than that with L-glucose, whereas the oxidation of two substrates resulted in similar morphologies for the AuNPs. As a control, the identical growth rate was observed for the oxidation of L-glucose and D-glucose (Supporting Information Figure S15), catalyzed by untreated AuNPs, which further illustrated the role of the capping DNA conformations in the chirality-based selective enlargement of the nanoparticles. Time-dependent absorbance changes of the catalytic enlarge-

DOI: 10.1021/cs5015805
ACS Catal. 2015, 5, 1489−1498

ment of AuNPs are shown in Figure 7C, indicating the substrate chirality- and ligands conformation-engineered growth rate.

Herein, one may raise such a concern that the DNA ligands may direct the catalytic deposition of Au^0 clusters along the helical grooves of DNA, resulting in the formation of a helical nanoparticle surface. If so, the chiral interactions among gold nanoparticle seeds, DNA, and glucose enantiomers, which accounted for the origin of the ligand and substrate chirality-dependent self-catalytic growth of the Au seeds, would be complicated. However, it is impossible that the helical nanoparticle surface occurred in the present system, for the following reasons:

First, the deposition of in-situ-generated Au^0 clusters (from reduction of $AuCl_4^-$ by H_2O_2) to the DNA ligand results from the coordination-based affinity of gold to the nitrogen atom of the DNA base, just like the noncovalent adsorption of DNA ligands to the catalytic AuNPs. If the DNA ligand were linked to nonmetallic surfaces, the in situ generated Au^0 clusters might interact with the DNA bases and deposit along the helical grooves of single- or double-stranded DNA ligands. However, in our case, many of the nitrogen atoms on the DNA ligands were already occupied by the catalytic AuNPs through coordination, which accounts for the formation of a chiral selective layer on the nanoparticles. Moreover, such coordination bonds were multivalent and strong. It is energetically disfavored that the in-situ-generated Au^0 reoccupied the coordinated nitrogen atoms on DNA bases. On the DNA-linking region of the nanoparticle surface, the in-situ-generated Au^0 clusters deposited on random positions of DNA strands are incapable of forming chirally arranged gold nanoclusters and helical nanoparticle surfaces. The deposition of Au^0 clusters was incapable of causing significant interference to the chiral interactions among the DNA ligand, glucose enantiomer substrates, and catalytic nanoparticles, which was the origin of the growth rate difference.

Second, it was reported that the asymmetrically shaped metallic or semiconductor nanoparticles exhibited detectable circular dichlorism (CD) signals at plasmonic wavelength,[63−67] and the chiral morphologies were observed by STEM (scanning transmission electron microscopy).[63,68,69] However, the enlarged AuNPs treated by ssDNA (**1**) or dsDNA (**1**)/(**2**) did not show any CD signals at the plasmonic absorption wavelength (Figure S16). It indicates there is no or a negligible amount of surface-linking DNA directing helical deposition of the in-situ-generated Au^0 clusters. Furthermore, we directly mixed different concentrations of H_2O_2 (1 or 20 μM) with ssDNA- or dsDNA-linked gold nanoparticles and $HAuCl_4$, resulting in different sizes and shapes of the enlarged gold seeds (Figure S17). Herein, 0.3 nM gold nanoparticles were pretreated by 3.0 μM DNA ligands, ensuring the gold nanoparticles were fully covered by DNA ligands. The gold nanoparticles showed very low GOx-mimicking catalytic activity at such high DNA ligands concentration (Figure 2) and were incapable of self-catalyzed growth because of low efficiency in producing H_2O_2. However, direct addition of H_2O_2 can enable the growth of the gold seeds by reduction of $HAuCl_4$. The deposition of in-situ-generated Au^0 clusters to DNA that covered gold nanoparticles with high grafting density would result in a higher yield of chiral gold nanostructures. Still, no CD signals were observed (Figure S18). On the other hand, the STEM images of the DNA-treated AuNPs that were enlarged by self-catalysis also did not show chiral morphologies (Figure S19).

On the issues of DNA−Au^0 interactions, CD signals, and chiral morphologies, DNA ligands treating the catalytic nanoparticles were incapable of directing the deposition of in-situ-generated Au^0 clusters into a helical configuration, which caused significant interference for the chiral interations among DNA ligand, glucose enantiomer substrates, and catalytic AuNP seeds.

Discussion. The recognition between DNA and glucose enantiomers played a vital role in the chirality-based selective catalysis of AuNPs, and DNA−glucose enantiomer interactions were strongly dependent on the DNA conformations. DNA in a randomly coiled state had a higher affinity to L-glucose, and structured DNA (duplex, i-motif, G-quadruplex) recognized D-glucose preferentially. DNA may interact with glucose through van der Waal forces and hydrogen bonding (sugar ring hydroxyl to N3 of the base).[31,43−45] The DNA random coil in the aqueous solution adopted a configuration of base stacking to minimize the benzene-like π-electron surface area, whereas the folded or hybridized DNA adopted the configuration with helical minor grooves between the bases. The simulated cavities that are provided by the structured DNA are indicated in Supporting Information Figure S20. With double-stranded DNA as the example, the docking of glucose into the DNA cavity can be described using the space-filling models of L-glucose and D-glucose. A shown in Figure S20, both glucose enantiomers adopt crescent shapes. In particular, the inherent bending of D-glucose geometrically complements the helical concaves of double-stranded DNA minor grooves more than L-glucose, through spatially oriented van der Waals interactions and hydrogen bonding. This is similar to the complementary fit of the dsDNA minor grooves to the oligosaccharide molecules, which were composed of D-glucose.[43−45] However, the monosaccharide cannot be compared with the oligosaccharide concerning multiple interactions with DNA and the molecular bending extent of the sterostructures, which may account for the limited selectivity of DNA-treated AuNPs. Although the detailed mechanism of DNA−glucose interactions is still unclear, it is reasoned that the molecular configuration of D-glucose prefers to bind with the grooves, which usually act as the binding sites, and L-glucose has a higher affinity with the stacked bases. The kinetic resolution is essentially based on stereoselective interactions.

CONCLUSIONS

In summary, this work introduced a proof of concept that used the multistimulated switchable nucleic ligands to engineer the catalytic chiral selectivity of metal nanoparticles toward the substrate enantiomers. DNA that adsorbed noncovalently to AuNPs acted as a chiral layer to confer the chiral differentiation to the catalytic AuNPs surface. Randomly coiled DNA-treated AuNPs showed higher catalytic activity toward L-glucose over D-glucose. The hybridization or folding of the capping DNA reversed the catalytic chiral selectivity of AuNPs. The DNA conformation-engineered chiral selectivity of AuNPs was also used to control the growth kinetics of the catalytic nanoparticle. ssDNA-treated AuNPs subjected to L-glucose showed a higher enlargement rate, whereas the growth rate of dsDNA−AuNPs exhibited a reversal dependence on the optical activity of the substrates. DNA-engineered chiral selectivity may also be employed in other reactions catalyzed by silver or platinum nanoparticles[70] through DNA adsorption. Smartly responsive catalytic systems can be enabled through introducing versatile external triggers (e.g., metal ions or light).[21,71] On the other hand, this work provides experimental evidence for the conformation-dependent chiral recognition of DNA to glucose, which can advance the understanding of the nucleic acid−

DOI: 10.1021/cs5015805
ACS Catal. 2015, 5, 1489−1498

saccharide (e.g., monosaccharide and polysaccharide) interactions that will be of biological significance.

■ ASSOCIATED CONTENT

Supporting Information

The following file is available free of charge on the ACS Publications website at DOI: 10.1021/cs5015805

Figures S1−S20

■ AUTHOR INFORMATION

Corresponding Authors

*E-mail: wangzg@nanoctr.cn.

*E-mail: dingbq@nanoctr.cn.

Notes

The authors declare no competing financial interest.

■ ACKNOWLEDGMENTS

The authors are grateful for financial support from the National Science Foundation China (21273052, 21173059, 91127021, and 21222311), National Basic Research Program of China (973 Program, 2012CB934000), and the 100-Talent Program of Chinese Academy of Sciences (B.Q.D).

■ REFERENCES

(1) Zhuo, C. X.; Zhang, W.; You, S. L. *Angew. Chem., Int. Ed.* **2012**, *51*, 12662−12686.

(2) Chen, M.; Roush, W. R. *J. Am. Chem. Soc.* **2012**, *134*, 10947−10952.

(3) Cooke, M. L.; Breit, B. *Angew. Chem., Int. Ed.* **2013**, *52*, 1890−1932.

(4) Silverio, D. L.; Torker, S.; Pilyugina, T.; Vieira, E. M.; Snapper, M. L.; Haeffner, F.; Hoveyda, A. H. *Nature* **2013**, *494*, 216−221.

(5) Laforteza, B. N.; Pickworth, M.; MacMillan, D. W. C. *Angew. Chem., Int. Ed.* **2013**, *52*, 11269−11272.

(6) Cockrell, J.; Wilhelmsen, C.; Rubin, H.; Martin, A.; Morgan, J. B. *Angew. Chem., Int. Ed.* **2012**, *51*, 9842−9845.

(7) Ito, H.; Kunii, S.; Sawamura, M. *Nat. Chem.* **2010**, *2*, 972−976.

(8) Watson, D. J.; Jesudason, R. J. B. R. J.; Beaumont, S. K.; Kyriakou, G.; Burton, J. W.; Lambert, R. M. *J. Am. Chem. Soc.* **2009**, *131*, 14584−14589.

(9) Wu, B.; Parquette, J. R.; RajanBabu, T. V. *Science* **2009**, *326*, 1662−1662.

(10) Zhou, S. L.; Fleischer, S.; Junge, K.; Das, S.; Addis, D.; Beller, M. *Angew. Chem., Int. Ed.* **2010**, *49*, 8121−8125.

(11) Schmidt, E.; Vargas, A.; Mallat, T.; Baiker, A. *J. Am. Chem. Soc.* **2009**, *131*, 12358−12367.

(12) Mallat, T.; Orglmeister, E.; Baiker, A. *Chem. Rev.* **2007**, *107*, 4863−4890.

(13) Tungler, A.; Sipos, E.; Hada, V. *Curr. Org. Chem.* **2006**, *10*, 1569−1583.

(14) Bartok, M. *Curr. Org. Chem.* **2006**, *10*, 1533−1567.

(15) Ward, D. E.; Becerril-Jimenez, F.; Zahedi, M. M. *J. Org. Chem.* **2009**, *74*, 4447−4454.

(16) Akai, Y.; Yamamoto, T.; Nagata, Y.; Ohmura, T.; Suginome, M. *J. Am. Chem. Soc.* **2012**, *134*, 11092−11095.

(17) Seeman, N. C. *Nano Lett.* **2010**, *10*, 1971−1978.

(18) Teller, C.; Willner, I. *Curr. Opin. Biotechnol.* **2010**, *21*, 376−391.

(19) Tan, L. H.; Xing, H.; Lu, Y. *Acc. Chem. Res.* **2014**, *47*, 1881−1890.

(20) Cho, E. J.; Lee, J. W.; Ellington, A. D. *Annu. Rev. Anal. Chem.* **2009**, *2*, 241−264.

(21) Clever, G. H.; Kaul, C.; Carell, T. *Angew. Chem., Int. Ed.* **2007**, *46*, 6226−6236.

(22) Ghosh, S.; Defrancq, E. *Chem.—Eur. J.* **2010**, *16*, 12780−12787.

(23) Kolpashchikov, D. M. *Chem. Rev.* **2010**, *110*, 4709−4723.

(24) Liu, D. S.; Balasubramanian, S. *Angew. Chem., Int. Ed.* **2003**, *42*, 5734−5736.

(25) Liu, H. J.; Xu, Y.; Li, F. Y.; Yang, Y.; Wang, W. X.; Song, Y. L.; Liu, D. S. *Angew. Chem., Int. Ed.* **2007**, *46*, 2515−2517.

(26) Lund, K.; Manzo, A. J.; Dabby, N.; Michelotti, N.; Johnson-Buck, A.; Nangreave, J.; Taylor, S.; Pei, R. J.; Stojanovic, M. N.; Walter, N. G.; Winfree, E.; Yan, H. *Nature* **2010**, *465*, 206−210.

(27) Goodman, R. P.; Heilemann, M.; Doose, S.; Erben, C. M.; Kapanidis, A. N.; Turberfield, A. J. *Nat. Nanotechnol.* **2008**, *3*, 93−96.

(28) Liu, J. W.; Cao, Z. H.; Lu, Y. *Chem. Rev.* **2009**, *109*, 1948−1998.

(29) Griffin, J. H.; Dervan, P. B. *J. Am. Chem. Soc.* **1986**, *108*, 5008−5009.

(30) Lin, P. H.; Tong, S. J.; Louis, S. R.; Chang, Y.; Chen, W. Y. *Phys. Chem. Chem. Phys.* **2009**, *11*, 9744−9750.

(31) Qu, X. G.; Trent, J. O.; Fokt, I.; Priebe, W.; Chaires, J. B. *Proc. Natl. Acad. Sci. U. S. A.* **2000**, *97*, 12032−12037.

(32) Yu, H. J.; Wang, X. H.; Fu, M. L.; Ren, J. S.; Qu, X. G. *Nucleic Acids Res.* **2008**, *36*, 5695−5703.

(33) Zhao, C. Q.; Ren, J. S.; Gregolinski, J.; Lisowski, J.; Qu, X. G. *Nucleic Acids Res.* **2012**, *40*, 8186−8196.

(34) Gan, H.; Tang, K. J.; Sun, T. L.; Hirtz, M.; Li, Y.; Chi, L. F.; Butz, S.; Fuchs, H. *Angew. Chem., Int. Ed.* **2009**, *48*, 5282−5286.

(35) Tang, K. J.; Gan, H.; Li, Y.; Chi, L. F.; Sun, T. L.; Fuchs, H. *J. Am. Chem. Soc.* **2008**, *130*, 11284−11285.

(36) Boersma, A. J.; Megens, R. P.; Feringa, B. L.; Roelfes, G. *Chem. Soc. Rev.* **2010**, *39*, 2083−2092.

(37) Roelfes, G.; Feringa, B. L. *Angew. Chem., Int. Ed.* **2005**, *44*, 3230−3232.

(38) Wang, C. H.; Jia, G. Q.; Zhou, J.; Li, Y. H.; Liu, Y.; Lu, S. M.; Li, C. *Angew. Chem., Int. Ed.* **2012**, *51*, 9352−9355.

(39) Li, H. X.; Rothberg, L. *Proc. Natl. Acad. Sci. U. S. A.* **2004**, *101*, 14036−14039.

(40) Zheng, X. X.; Liu, Q.; Jing, C.; Li, Y.; Li, D.; Luo, W. J.; Wen, Y. Q.; He, Y.; Huang, Q.; Long, Y. T.; Fan, C. H. *Angew. Chem., Int. Ed.* **2011**, *50*, 11994−11998.

(41) Comotti, M.; Della Pina, C.; Matarrese, R.; Rossi, M. *Angew. Chem., Int. Ed.* **2004**, *43*, 5812−5815.

(42) Pei, H.; Li, F.; Wan, Y.; Wei, M.; Liu, H. J.; Su, Y.; Chen, N.; Huang, Q.; Fan, C. H. *J. Am. Chem. Soc.* **2012**, *134*, 11876−11879.

(43) Arya, D. P. *Acc. Chem. Res.* **2011**, *44*, 134−146.

(44) Krishna, A. G.; Balasubramanian, D.; Ganesh, K. N. *Biochem. Biophys. Res. Commun.* **1994**, *202*, 204−210.

(45) Ikemoto, N.; Kumar, R. A.; Ling, T. T.; Ellestad, G. A.; Danishefsky, S. J.; Patel, D. J. *Proc. Natl. Acad. Sci. U. S. A.* **1995**, *92*, 10506−10510.

(46) Wei, H.; Wang, E. K. *Chem. Soc. Rev.* **2013**, *42*, 6060−6093.

(47) Denard, C. A.; Hartwig, J. F.; Zhao, H. M. *ACS Catal.* **2013**, *3*, 2856−2864.

(48) Ziegler, C.; Eychmuller, A. *J. Phys. Chem. C* **2011**, *115*, 4502−4506.

(49) Demers, L. M.; Mirkin, C. A.; Mucic, R. C.; Reynolds, R. A.; Letsinger, R. L.; Elghanian, R.; Viswanadham, G. *Anal. Chem.* **2000**, *72*, 5535−5541.

(50) Zhang, X.; Servos, M. R.; Liu, J. W. *Langmuir* **2012**, *28*, 3896−3902.

(51) Zhan, P. F.; Wang, J. Y.; Wang, Z. G.; Ding, B. Q. *Small* **2014**, *10*, 399−406.

(52) Lepecq, J. B.; Paoletti, C. *J. Mol. Biol.* **1967**, *27*, 87−&.

(53) Wang, K.; Zhang, Z.; Guo, Q. N.; Bao, X. P.; Li, Z. Y. *Acta Chim. Sin.* **2007**, *65*, 2597−2603.

(54) Zheng, D. M.; Zou, R. X.; Lou, X. H. *Anal. Chem.* **2012**, *84*, 3554−3560.

(55) Nagatoishi, S.; Nojima, T.; Galezowska, E.; Juskowiak, B.; Takenaka, S. *ChemBioChem.* **2006**, *7*, 1730−1737.

(56) Shim, J. W.; Tan, Q. L.; Gu, L. Q. *Nucleic Acids Res.* **2009**, *37*, 972−982.

(57) Wang, Z. D.; Tang, L. H.; Tan, L. H.; Li, J. H.; Lu, Y. *Angew. Chem., Int. Ed.* **2012**, *51*, 9078−9082.

(58) Langille, M. R.; Zhang, J. A.; Mirkin, C. A. *Angew. Chem., Int. Ed.* **2011**, *50*, 3543−3547.

DOI: 10.1021/cs5015805
ACS Catal. 2015, 5, 1489−1498

(59) Xue, C.; Mirkin, C. A. *Angew. Chem., Int. Ed.* **2007**, *46*, 2036−2038.
(60) Zhu, C.; Zeng, J.; Tao, J.; Johnson, M. C.; Schmidt-Krey, I.; Blubaugh, L.; Zhu, Y. M.; Gu, Z. Z.; Xia, Y. N. *J. Am. Chem. Soc.* **2012**, *134*, 15822−15831.
(61) Willner, I.; Baron, R.; Willner, B. *Adv. Mater.* **2006**, *18*, 1109−1120.
(62) Luo, W. J.; Zhu, C. F.; Su, S.; Li, D.; He, Y.; Huang, Q.; Fan, C. H. *ACS Nano* **2010**, *4*, 7451−7458.
(63) Yeom, J.; Yeom, B.; Chan, H.; Smith, K. W.; Dominguez-Medina, S.; Bahng, J. H.; Zhao, G. P.; Chang, W. S.; Chang, S. J.; Chuvilin, A.; Melnikau, D.; Rogach, A. L.; Zhang, P. J.; Link, S.; Král, P.; Kotov, N. A. *Nat. Mater.* **2015**, *14*, 66−72.
(64) Maoz, B. M.; van der Weegen, R.; Fan, Z. Y.; Govorov, A. O.; Ellestad, G.; Berova, N.; Meijer, E. W.; Markovich, G. *J. Am. Chem. Soc.* **2012**, *134*, 17807−17813.
(65) Shemer, G.; Krichevski, O.; Markovich, G.; Molotsky, T.; Lubitz, I.; Kotlyar, A. B. *J. Am. Chem. Soc.* **2006**, *128*, 11006−11007.
(66) Petty, J. T.; Zheng, J.; Hud, N. V.; Dickson, R. M. *J. Am. Chem. Soc.* **2004**, *126*, 5207−5212.
(67) Santizo, I. E.; Hidalgo, F.; Perez, L. A.; Noguez, C.; Garzon, I. L. *J. Phys. Chem. C* **2008**, *112*, 17533−17539.
(68) Gerbier, P.; Domingo, N.; Gomez-Segura, J.; Ruiz-Molina, D.; Amabilino, D. B.; Tejada, J.; Williamson, B. E.; Veciana, J. *J. Mater. Chem.* **2004**, *14*, 2455−2460.
(69) Wang, Z. W.; Palmer, R. E. *Nano Lett.* **2012**, *12*, 5510−5514.
(70) Yang, J.; Lee, J. Y.; Too, H. P.; Chow, G. M. *Biophys. Chem.* **2006**, *120*, 87−95.
(71) Kang, H. Z.; Liu, H. P.; Phillips, J. A.; Cao, Z. H.; Kim, Y.; Chen, Y.; Yang, Z. Y.; Li, J. W.; Tan, W. H. *Nano Lett.* **2009**, *9*, 2690−2696.

DOI: 10.1021/cs5015805
ACS Catal. 2015, 5, 1489−1498